Imaging in scattering media by use of laser speckle

C. A. Thompson,* K. J. Webb, and A. M. Weiner

School of Electrical and Computer Engineering, Purdue University, West Lafayette, Indiana 47907-1285

Received October 11, 1996; revised manuscript received March 10, 1997; accepted March 4, 1997

We present a method for the detection and localization of inhomogeneities embedded within highly scattering media that employs speckle statistics with a partially coherent light source. Variations in speckle contrast as a function of position are used to interrogate inhomogeneities deeply embedded within scattering media. A numerical model based on photon diffusion theory is introduced to predict speckle contrast as a function of scan position. This model uses measured speckle data to determine scattering and absorption parameters.
© 1997 Optical Society of America [S0740-3232(97)03309-7]

1. INTRODUCTION

Optical imaging within and through scattering media is of interest in biological and remote-sensing applications. For example, the reliable early detection of soft-tissue tumors by optical means would be an important medical breakthrough. With materials that are thick relative to the mean free path between scattering events, it becomes unrealistic to perform geometric holography based on the coherent properties of light. With thin or lightly scattering materials, frequency and time gating techniques have been used successfully.[1–3] For highly scattering materials a variety of incoherent light techniques have been presented that provide inhomogeneity localization based on a diffusion equation model for the light; hence their categorization as optical diffusion imaging approaches.[4–6] Based on this diffusion equation model, efforts have been made to inversely calculate inhomogeneity size and location.[7]

Attempts are frequently made to reduce laser speckle noise when an image is being formed. There are, however, a variety of uses for laser speckle. It has been shown that laser speckle can provide information on target separation in a turbulent atmosphere (imaging correlography).[8] Several examples have been shown in which a temporal intensity decorrelation[9,10] or difference[11,12] of laser speckle provides information on material movement such as blood circulation or growth. Speckle contrast has been used in the optical characterization of surface roughness.[13] Similarly, it has been shown that speckle contrast is useful in detecting skin disease in lightly scattering, thin samples.[14] A relation between the intensity correlation and the time evolution of speckle in an optically changing random medium has been shown.[15] A theoretical study of limitations in making high-resolution paraxial images of objects lying behind an optically turbid medium concluded that the transmission of image information is strongly dependent on the exit pupil size and the photon mean free path.[16] An empirical relation between the intensity autocorrelation over frequency and the thickness of thin diffuse samples has been shown,[17] suggesting that imaging a speckle spot could be the basis of determining the diffusion coefficient. In this experiment a laser line was scanned over frequencies up to 30 GHz and the intensity measured over a small area (the size of a speckle spot). The intensity in the image spot varied with frequency because of the frequency-dependent coherent superposition of light that traversed many paths. The thicker the sample, the more rapid the variation of intensity with frequency and the smaller the frequency-correlation width. Similar intensity-correlation results have been demonstrated for the case of pulse illumination, in which the diffusion equation model was shown to be a good fit to the temporal distribution.[18]

In this paper we propose and provide experimental evidence for a method of determining the location of an inhomogeneity embedded within a highly scattering medium by use of laser speckle. In particular, we use the speckle contrast as a function of scan position to identify the presence of an inhomogeneity, assuming a time-invariant measurement domain. The numerical solution of the photon diffusion equation provides a forward model for the contrast ratio. The diffusion model assumes that there is appreciable scattering, i.e., that the material thickness is more than approximately three times the mean free path. Inversion techniques then provide the optical scattering parameters for the background and inhomogeneity. The approach relies on using light with a coherence length comparable to the standard deviation of path lengths through a scattering medium. We recently introduced the concept of using speckle contrast to characterize scattering materials.[19] The speckle contrast serves as a metric that describes the amount of scatter and absorption that photons experience while traversing diffuse media. For example, with nonzero optical bandwidth, a thicker or more highly scattering medium results in a lower speckle contrast ratio. An analytic diffusion equation model was developed to allow the determination of scattering and absorption parameters (μ_s' and μ_a) from measured speckle contrast as a function of material thickness. We also showed that longitudinally inhomogeneous slabs that have a sandwich arrangement can be

 © 1997 Optical Society of America

differentiated on the basis of speckle contrast. Here we extend the concept by looking at a scanning arrangement that provides imaging data for two-dimensional inhomogeneities. Such inhomogeneous problems require a numerical solution of the diffusion equation.

The speckle contrast ratio is defined as σ_I/μ_I, where σ_I is the standard deviation and μ_I is the average of the light intensity over the speckle pattern. In a situation in which the light is perfectly coherent, the speckle contrast maintains a value of one once there is sufficient scatter. However, if the light is partially coherent, the speckle contrast can have a value somewhere between zero and one, depending on the coherence of the source and the degree of scatter experienced by the light.[20] As the light becomes less coherent, the probability density for intensity approaches a delta function at the mean value. For greatest effectiveness it is necessary that the spread in travel path lengths of detected photons leaving a diffuse medium (the characteristic length, which we define as the standard deviation of the distribution, σ_l) be of the same order as the coherence length of the source, l_c. It should be noted that if $\sigma_l \ll l_c$ the contrast approaches one (perfectly coherent case) and when $\sigma_l \gg l_c$ the contrast tends toward zero (incoherent case).

A description of the first-order speckle statistics that uses a contrast ratio is developed in terms of the probability-density function for path length through the medium. This probability density is a function of the material scattering parameters and is obtained by use of a numerical solution to the diffusion equation. Measured contrast ratio data as a function of scan position for several geometries support the model and our contention that the approach provides imaging capabilities.

2. SPECKLE STATISTICS

Consider the transmission of light through a scattering medium and the imaging of this light at the output planar surface (at $z = z_i$) over a small domain, an image spot centered at (x_{i0}, y_{i0}), with z the axial direction (which is the same as the propagation direction of the incident light) and (x_i, y_i) the transverse coordinates on the image plane. The incident optical power spectral density is $S(\lambda)$ W/m^3, so the power density is

$$I_{\text{inc}} = \int_0^\infty S(\lambda)\mathrm{d}\lambda. \tag{1}$$

I_{inc} is a function of position within the illumination spot of an incident laser beam, and its integral over space gives the total incident power. The spatial support of the incident laser beam in our experiments is small, approaching a point source, relative to that for the light at the output surface of a highly scattering medium.

With a large number of random scattering events, the complex field spectral amplitude at each point in the image plane at wavelength λ,

$$U(x_i, y_i, \lambda) = U_r(x_i, y_i, \lambda) + iU_i(x_i, y_i, \lambda), \tag{2}$$

has a real part U_r and an imaginary part U_i with a Gaussian probability-density function with zero mean, which are uncorrelated in the limit as the number of scattering events increases. In polar form, the random field becomes

$$U(x_i, y_i, \lambda) = U_m(x_i, y_i, \lambda)\exp[-i\phi(x_i, y_i, \lambda)], \tag{3}$$

where U_m is the field magnitude random variable, which has a Rayleigh density if U_r and U_i are Gaussian, and ϕ is the random phase, which has a uniform density if the standard deviation of the path lengths through the medium is large relative to the wavelength ($\sigma_l \gg \lambda$), which we assume to be the case for a heavily scattering medium. If U_r and U_i are independent, it follows that U_m and ϕ are also.

Note that when we assume independent Gaussian statistics for the fields, we are assuming a large number of scattering events. As the number of scattering events approaches infinity, with a source of noninfinite coherence length, the speckle contrast will approach zero. We are interested in a regime in which the degree of scatter is sufficient for the Gaussian model to hold but not large enough to wash out the speckle completely.

Let

$$\begin{aligned} U_m{}^2(x_i, y_i, \lambda) &= S(\lambda)I_n(x_i, y_i, \lambda) \\ &= I(x_i, y_i, \lambda), \end{aligned} \tag{4}$$

where I_n is the normalized intensity random variable, which is defined as the intensity at the image plane point (x_i, y_i) with $S(\lambda) = 1$. I_n is a function of wavelength over broad wavelength ranges but not over the bandwidth of a relatively narrow-band laser, because the medium scattering parameters are usually a weak function of wavelength. For monochromatic speckle the intensity probability-density function has a negative exponential form given by

$$p(I, \lambda) = \frac{1}{2\pi\sigma_I{}^2}\exp[-I/(2\sigma_I{}^2)], \tag{5}$$

where $\sigma_I{}^2$ is the variance.

The phase in Eq. (3) can be described in terms of a path-length random variable l, where

$$\phi(x_i, y_i, \lambda) = (2\pi/\lambda)l(x_i, y_i). \tag{6}$$

Note that we assume in Eq. (6) a sufficiently high light coherence that the medium parameters, including l, are independent of λ.

When the observation time is large relative to the coherence time of the light,[21] the expected value of intensity ($\mu_I = \langle I\rangle$) can be expressed as the incoherent superposition

$$\langle I(x_i, y_i)\rangle = \int_0^\infty S(\lambda)\langle I_n(x_i, y_i, \lambda)\rangle\mathrm{d}\lambda. \tag{7}$$

In Eq. (7), $\langle I_n(x_i, y_i, \lambda)\rangle$ is the expected value of the normalized intensity at wavelength λ, given by

$$\langle I_n(x_i, y_i, \lambda)\rangle = \int_0^\infty I_n(x_i, y_i, \lambda)p(I, \lambda)\mathrm{d}I, \tag{8}$$

where $p(I, \lambda)$ is the density function for intensity at a single λ, given by Eq. (5). The second moment of $I(x_i, y_i)$ can be expressed as

$$\langle I^2(x_i, y_i)\rangle = \int_0^\infty \int_0^\infty S(\lambda)S(\lambda')\langle I_n(x_i, y_i, \lambda) \times I_n(x_i, y_i, \lambda')\rangle \mathrm{d}\lambda \mathrm{d}\lambda'. \quad (9)$$

In Eq. (9) the normalized first-order intensity autocorrelation is

$$\Gamma_I(\lambda, \lambda') = \langle I_n(x_i, y_i, \lambda) I_n(x_i, y_i, \lambda')\rangle. \quad (10)$$

Equation (9) can be evaluated as the limiting value of the second-order statistics for the second moment of intensity, given by

$$\langle I(x_i, y_i) I(x_i', y_i')\rangle = \int_0^\infty \int_0^\infty S(\lambda)S(\lambda')\langle I_n(x_i, y_i, \lambda) \times I_n(x_i', y_i', \lambda')\rangle \mathrm{d}\lambda \mathrm{d}\lambda'. \quad (11)$$

Expanding the expected quantity in the integrand of Eq. (11) in terms of the normalized complex field U_n, where $I_n(x_i, y_i, \lambda) = U_n(x_i, y_i, \lambda) U_n^*(x_i, y_i, \lambda)$, gives

$$\langle I_n(x_i, y_i, \lambda) I_n(x_i', y_i', \lambda')\rangle = \langle U_n(x_i, y_i, \lambda) U_n^*(x_i, y_i, \lambda) \times U_n(x_i', y_i', \lambda') U_n^*(x_i', y_i', \lambda')\rangle. \quad (12)$$

For w_i a complex Gaussian process,[22]

$$\langle w_1^* w_2^* w_3 w_4\rangle = \langle w_1^* w_3\rangle\langle w_2^* w_4\rangle + \langle w_2^* w_3\rangle\langle w_1^* w_4\rangle. \quad (13)$$

Using Eq. (13), we can write Eq. (12) as

$$\langle I_n(x_i, y_i, \lambda) I_n(x_i', y_i', \lambda')\rangle = \langle I_n(x_i, y_i, \lambda)\rangle\langle I_n(x_i', y_i', \lambda')\rangle + |\langle U_n(x_i, y_i, \lambda) U_n^*(x_i', y_i', \lambda')\rangle|^2. \quad (14)$$

The variance in the first-order intensity statistics, $\sigma_I^2(x_i, y_i) = \langle I^2(x_i, y_i)\rangle - \langle I(x_i, y_i)\rangle^2$, from Eqs. (7), (9), and (14), with $x_i = x_i'$ and $y_i = y_i'$, becomes

$$\sigma_I^2(x_i, y_i) = \int_0^\infty \int_0^\infty S(\lambda)S(\lambda')|\langle U_n(x_i, y_i, \lambda) \times U_n^*(x_i, y_i, \lambda')\rangle|^2 \mathrm{d}\lambda \mathrm{d}\lambda'. \quad (15)$$

Consider that the image spot centered at (x_{i0}, y_{i0}) is small enough for μ_I and σ_I to be constant yet large enough relative to the speckle size to represent an adequate statistical sample space. The values of μ_I and σ_I will in general be a function of scan position (x_{i0}, y_{i0}). At (x_{i0}, y_{i0}), from Eqs. (3) and (15),

$$\sigma_I^2 = \int_0^\infty \int_0^\infty S(\lambda)S(\lambda')|\langle I_n^{1/2}(\lambda) I_n^{1/2}(\lambda') \times \exp\{-i[\phi(\lambda) - \phi(\lambda')]\}\rangle|^2 \mathrm{d}\lambda \mathrm{d}\lambda'. \quad (16)$$

As we have assumed that U_m and ϕ are independent,

$$\sigma_I^2 = \int_0^\infty \int_0^\infty S(\lambda)S(\lambda')|\langle I_n^{1/2}(\lambda) I_n^{1/2}(\lambda')\rangle|^2 \times |\langle \exp\{-i[\phi(\lambda) - \phi(\lambda')]\}\rangle|^2 \mathrm{d}\lambda \mathrm{d}\lambda' = \int_0^\infty \int_0^\infty S(\lambda)S(\lambda')|\Gamma_U(\lambda, \lambda')|^2 \mathrm{d}\lambda \mathrm{d}\lambda', \quad (17)$$

where Γ_U is the normalized autocorrelation function of the field spectrum given by $\langle U_n(\lambda) U_n^*(\lambda')\rangle$. Consider a coherence restriction where the bandwidth given by $S(\lambda)$ is sufficiently small that the scattering medium properties are independent of λ, so we write

$$\langle I_n(\lambda)\rangle = I_0, \quad (18)$$

where I_0 is a constant over the integration range in Eq. (17). Substituting Eq. (6) into Eq. (17) gives

$$\sigma_I^2 = I_0^2 \int_0^\infty \int_0^\infty S(\lambda)S(\lambda') \times \left|\left\langle \exp\left[-i2\pi l\left(\frac{1}{\lambda} - \frac{1}{\lambda'}\right)\right]\right\rangle\right|^2 \mathrm{d}\lambda \mathrm{d}\lambda'. \quad (19)$$

From Eq. (7),

$$\mu_I = I_0 \int_0^\infty S(\lambda) \mathrm{d}\lambda. \quad (20)$$

Therefore, as a function of scan position (x_{i0}, y_{i0}), the contrast ratio becomes

$$\frac{\sigma_I}{\mu_I}(x_{i0}, y_{i0}) = \left\{ \int_0^\infty \int_0^\infty S(\lambda)S(\lambda') \times \left|\left\langle \exp\left[-i2\pi l\left(\frac{1}{\lambda} - \frac{1}{\lambda'}\right)\right]\right\rangle\right|^2 \mathrm{d}\lambda \mathrm{d}\lambda' \right\}^{1/2} \Big/ \int_0^\infty S(\lambda) \mathrm{d}\lambda. \quad (21)$$

Note the dependence of σ_I/μ_I in Eq. (21) on the coherence length of the light source, $l_c \sim \lambda^2/\Delta\lambda$, where the bandwidth $\Delta\lambda$ is implied in the exponential through the integration range defined by $S(\lambda)$. The expected value of the phase term, or characteristic function, in Eq. (21) is

$$\left\langle \exp\left[-i2\pi l\left(\frac{1}{\lambda} - \frac{1}{\lambda'}\right)\right]\right\rangle = \int_0^\infty p(l) \exp\left[-i2\pi l\left(\frac{1}{\lambda} - \frac{1}{\lambda'}\right)\right] \mathrm{d}l, \quad (22)$$

where $p(l)$ is the probability-density function for the path length. With a change of variable, Eq. (22) is the Fourier transform of $p(l)$.

An image cannot be recorded precisely at the output of the scattering medium but rather is formed through collection optics to form an image on, for example, a CCD camera. The influence of the imaging optical system can be represented in terms of the point-spread function. The detected field (at the CCD camera) can be written as

$$U_d(x, y, \lambda) = U(x_i, y_i, \lambda) * K(x, y, x_i, y_i, \lambda), \quad (23)$$

where K is the point-spread function or Green's function. In Appendix A we derive the contrast ratio at the (CCD) detector plane. It is shown that, provided that μ_I and σ_I are constant over the small spot at (x_i, y_i) and that all light other than from this spot is rejected from the image formed at the detector plane, the contrast ratio at the image spot will be identical to that measured at the detector plane. With these assumptions, the contrast ratio in Eq. (21) can therefore be applied directly to the measured speckle intensity statistics. Qualitatively, this is satisfying because of the deterministic nature of the imaging system.

The requirement of a model for optical scattering in a material is to relate material parameters to a measured contrast ratio in Eq. (21) through $p(l)$ in Eq. (22). Diffusion theory provides that model in this heavily scattering context.

3. DIFFUSION MODEL

We assume that there is appreciable scatter in the medium so that particle transport theory can be used to describe the light. In particular, we consider the diffusion equation approximation to the Boltzmann transport equation[4–6] to determine $p(l)$ in Eq. (22). The intent is to use this diffusion equation representation to describe the time envelope for the light transport to each point on the output surface of the scattering material. We assume that this model can be used as a basis for determining a length or time-density function in terms of the optical scattering and absorption parameters of the medium. Clearly, a particle model cannot be used to describe the coherent fields, but we have shown that it is a good measure of the statistics of a partially coherent field when there is appreciable scatter.[19]

The diffusion equation in a homogeneous region is[4,5]

$$\frac{1}{c}\frac{\partial}{\partial t}\Phi(\mathbf{r}, t) - D\nabla^2\Phi(\mathbf{r}, t) + \mu_a\Phi(\mathbf{r}, t) = Q(\mathbf{r}, t), \tag{24}$$

where c is the speed of light between scattering events, $\Phi(\mathbf{r}, t)$ is the radiative flux (sometimes referred to as the photon fluence rate) in watts per square centimeter at position $\mathbf{r} = x\hat{\mathbf{x}} + y\hat{\mathbf{y}} + z\hat{\mathbf{z}}$ at time t. Q is the source (W/cm^3) and D is the diffusion coefficient (cm), defined as $D = [3(\mu_a + \mu_s')]^{-1}$, where μ_a is the linear absorption coefficient (cm^{-1}), $\mu_s' = (1 - g)\mu_s$ is the reduced scattering coefficient (cm^{-1}), μ_s is the linear scattering coefficient (cm^{-1}), and g is the mean cosine of the scattering angle.

The light leaving the material as a function of position is given by Fick's law as[6]

$$T(\mathbf{r}, t) = \hat{\mathbf{n}} \cdot [-D\nabla\Phi(\mathbf{r}, t)], \tag{25}$$

where $\mathbf{J} = -D\nabla\Phi$ is the photon current density and $\hat{\mathbf{n}}$ is the outward normal. Consider solving Eq. (24) for $\Phi(x', 0, d)$ for a material of thickness $z = d$ with a source given by $Q(x, y, z, t) = \delta(x - x')\delta(y)\delta(z - z')\delta(t)$. As x' is changed, which corresponds to scanning the source point along the x axis, the observation point is also scanned to be directly opposite on the output face of the domain. Substituting $t = l/c$ into Eq. (25) and normalizing results in

$$p(l) = \frac{T(x', y, z, l/c)}{\int_0^\infty T(x', y, z, l/c)\mathrm{d}l}. \tag{26}$$

Equation (26) is the probability-density function for photon path length that is used in Eqs. (22) and (21).

Equation (24), and hence $p(l)$ in Eq. (26), can be evaluated analytically for homogeneous problems in which the Green's function can be used or for simple geometries in which a satisfactory approximate solution can be found. In our previous work with a homogeneous slab we used image theory to determine an analytic solution for $p(l)$.[19] The image sources were introduced to form a Dirichlet boundary condition ($\Phi = 0$) on extrapolated boundaries, which has been shown to be a good representation of the physical problem. With a view to imaging inhomogeneities, we address the general numerical solution of Eq. (24).

We have modified the public-domain three-dimensional multigrid finite-difference partial differential equation solver MUDPACK[23,24] to solve the time-dependent diffusion equation in four dimensions (three spatial dimensions and one temporal dimension). The fourth dimension is incorporated by use of an implicit finite-difference scheme. In Cartesian coordinates, Eq. (24) becomes

$$D\left(\frac{\partial^2\Phi_{n+1}}{\partial x^2} + \frac{\partial^2\Phi_{n+1}}{\partial y^2} + \frac{\partial^2\Phi_{n+1}}{\partial z^2}\right) - \left(\mu_a + \frac{1}{c}\frac{1}{\Delta t}\right)\Phi_{n+1} = -Q - \frac{1}{c}\frac{1}{\Delta t}\Phi_n. \tag{27}$$

MUDPACK can be used to solve Eq. (27) for Φ at each time step, which subsequently becomes the right-hand side at the next time step. A point source Q exists for one time step at a grid point located one transport mean free path ($3D$) inside the medium. Physically, this is the average distance that a photon travels unscattered, and therefore it is reasonable to assume an equivalent point source for the diffusion equation at this location.

In the representation of Eq. (27) the homogeneous diffusion equation is solved numerically in locally homogeneous regions. It has been assumed that $\nabla D \cdot \nabla\Phi = 0$, which results in a small boundary condition error between regions of differing μ_a and μ_s'. For the geometry considered here, with a more highly scattering inhomogeneity, the maximum error in σ_l due to this assumption is 3.6%.

An approximate boundary condition for the diffusion equation must be used at the interface with the nonscattering (free-space) external region. Consider a boundary condition $\Phi = 0$ on an extrapolated boundary (outside the medium), which is equivalent to assuming that there is only an outward photon current.[6] This boundary condition has been improved slightly by use of empirical results by representing the mismatched refractive indices. Consider light diffusing out of a volume with a refractive index of n and into air ($n_{\mathrm{air}} = 1$). At the interface, the total diffuse photon current density reflected back into

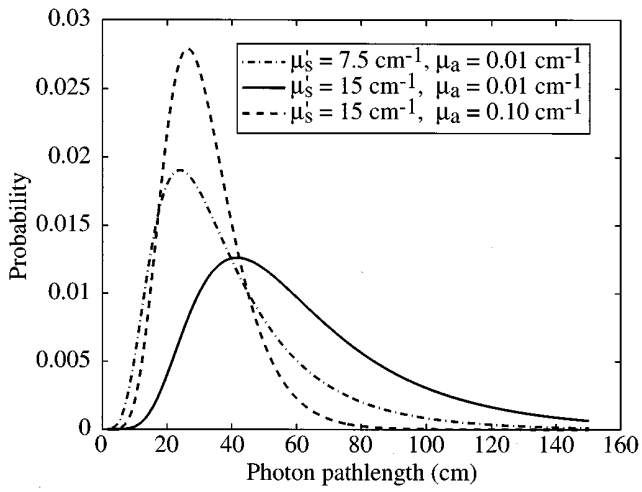

Fig. 1. Normalized impulse responses or path-length probability-density functions for three different sets of scattering and absorption parameters for a slab of thickness 3.6 cm.

the medium, J_{in}, is a percentage (r_d) of the current density leaving the medium, J_{out}, written as[25,26]

$$J_{\text{in}} = r_d J_{\text{out}}. \tag{28}$$

Consider, for example, an interface plane at $z = z_s$. Using Fick's law, we can express Eq. (28) as

$$\Phi(x_s, y_s, z_s, t) - \frac{D}{2} \left.\frac{\partial \Phi(x_s, y_s, z, t)}{\partial z}\right|_{z=z_s} = r_d \left[\Phi(x_s, y_s, z_s, t) + \frac{D}{2} \left.\frac{\partial \Phi(x_s, y_s, z, t)}{\partial z}\right|_{z=z_s} \right], \tag{29}$$

where the subscript s signifies coordinates on a surface that is normal to z. Equation (29) can be written as

$$\left(\frac{1 - r_d}{1 + r_d}\right) \frac{1}{2D} \Phi(x_s, y_s, z_s, t) - \left.\frac{\partial \Phi(x_s, y_s, z, t)}{\partial z}\right|_{z=z_s} = 0. \tag{30}$$

The form of Eq. (30) is such that it can be placed directly in the MUDPACK code as the boundary condition. For the case of a diffuse wave at the surface of a mismatched boundary, Egan and Hilgeman[26] have shown a reflectance function of the form[25]

$$r_d = 0.0636n + 0.6681 + 0.7099n^{-1} - 1.4399n^{-2}, \tag{31}$$

achieved empirically by curve fitting data presented by Orchard.[27] In Eq. (31), n is the normalized refractive index of the medium, $n = n_1/n_2$, which becomes the refractive index for the medium at a free-space boundary. We have independently verified the form of this function against Orchard's data. Previously we used Eqs. (30) and (31) to determine an analytic solution for the diffusion equation.[19] The same boundary conditions are used here in the finite-difference solution.

Figure 1 shows normalized impulse responses corresponding to the photon path lengths (travel time if the ordinate is scaled by $1/c$) through three samples of 3.6 cm thickness with scattering characteristics of $\mu_a = 0.01$ cm^{-1}, $\mu_s' = 7.5$ cm^{-1}; $\mu_a = 0.01$ cm^{-1}, $\mu_s' = 15.0$ cm^{-1}; and $\mu_a = 0.10$ cm^{-1}, $\mu_s' = 15.0$ cm^{-1}. From Fig. 1 the influence of the various scattering parameters on the shape of the impulse response is apparent. Note that a larger μ_s' tends to increase the length of the standard deviation or the characteristic length σ_l, whereas a larger μ_a tends to reduce σ_l. When σ_l is of the same order of magnitude as the coherence length of the laser source l_c, the speckle contrast will be most sensitive to material variations. The characteristic path lengths in Fig. 1 are approximately 22.43, 28.18 cm, and 12.23 cm (for the order given in the legend), respectively, which are close to the free-space (approximately 22-cm) coherence length of a typical long-cavity (≈1-m) He–Ne laser.

Once the length probability-density function $p(l)$ is determined for a particular μ_a and μ_s', Eq. (21) is integrated to give a numerically calculated value of speckle contrast. The values of μ_a and μ_s' can be determined iteratively by fitting a measured σ_I/μ_I as a function of a distance variable.

4. EXPERIMENT

The goal is to locate inhomogeneities, i.e., the presence of regions with differing μ_a and μ_s' from the background within a scattering medium. The following experiment was conducted to determine whether speckle could be used to detect such inhomogeneities.

A 3.6 cm × 15 cm × 15 cm diffuse medium was assembled with white Plexiglas ($\mu_a \approx 0.01$ cm^{-1}, $\mu_s' \approx 15$ cm^{-1}).[19] A more optically scattering 1.2 cm × 1.8 cm × 15 cm white Plexiglas inhomogeneity was embedded within the material ($\mu_a \approx 0.005$ cm^{-1}, $\mu_s' \approx 40.0$ cm^{-1}),[19] as shown in Fig. 2. The plastic assembly was mounted on a translational stage so that it could be scanned across the source–detector pair. In this scanning arrangement the source and the detector are fixed relative to each other and the plastic is moved, so for modeling purposes this corresponds to varying x' in Eq. (26), and $z = d$ (=3.6 cm) defines the output surface.

Figure 3 is a schematic diagram of the imaging system that we used to perform the experiment. A laser beam from a 632.8-nm cw He–Ne laser was used as the illumi-

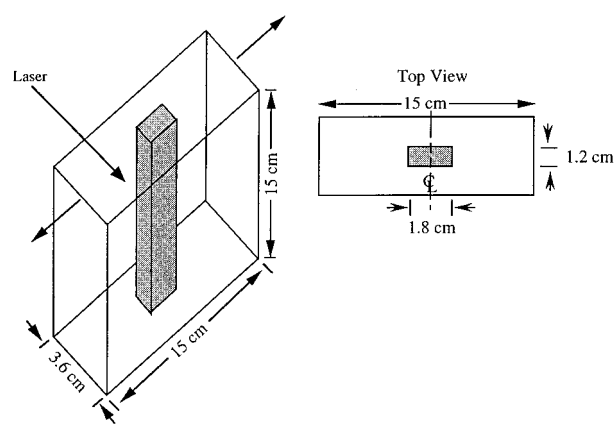

Fig. 2. Diagram of the scattering medium with embedded inhomogeneity. Note that scanning implies that the plastic is scanned with a fixed source and detector.

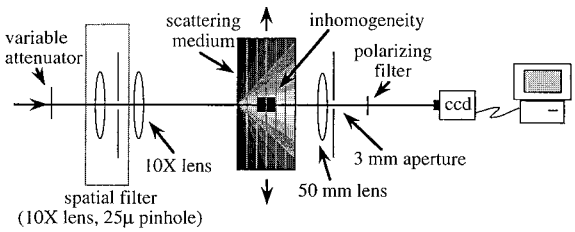

Fig. 3. Experimental arrangement for speckle measurements.

nation source. The laser line was measured to have an approximate FWHM linewidth of 900 MHz (with a mode spacing of 161 MHz). The incident light was spatially filtered and collimated to a beam radius of approximately 1 mm before impinging upon the plastic. The laser beam was scattered by the plastics, and the resulting speckle pattern was passed through a polarizer and then imaged onto a CCD array. The aperture between the imaging lens and the polarizer was used to control the speckle size; both adequate pixel resolution of the speckle and a sufficient number of spots over the image domain for good statistics were necessary. Reducing the aperture increased the speckle size. The imaged area on the output face of the plastic was approximately 1 mm by 1 mm. Experiments were performed with minimal ambient light to preclude the effects of other sources. The image formed on the CCD camera was sent to a personal computer via an 8-bit frame-grabber card. The CCD camera exhibited nonlinearity as a function of optical intensity. Therefore, during the postprocessing, raw data from the CCD camera were linearized before statistical analysis. We obtained the transformation required for linearization by recording CCD camera intensity levels, using a LED source (with low coherence for uniform illumination) while changing neutral-density filters to attenuate the light.

The uniformity of the intensity statistics obtained by using different portions of the CCD camera image was investigated. The mean and the standard deviation for the images were approximately uniform, and the contrast ratio for the various test regions varied by less than $\pm 2.6\%$. This variation could be due to quantization error coupled with statistical noise. The camera had 480×640 pixels, of which the last four rows and the first column were dark. These dark pixels will skew the absolute scattering parameter values slightly (approximately a 3% change in contrast ratio) but will not alter the relative spatially dependent effects observed.

Figure 4 shows the experimental intensity contrast ratio (σ_I/μ_I) data achieved in two runs with the more highly scattering plastic embedded in the less scattering white Plexiglas background. The two data sets were taken sequentially, i.e., the data for one experimental curve were obtained and then the scan was repeated and another data set collected. Note that the contrast ratio is lowest when the source and the detector are opposite the more highly scattering inhomogeneity. Conceptually, when the bulk of the photons pass through the more highly scattering medium, the speckle contrast will be small. As the object is translated and the dense inhomogeneity is no longer centered, the speckle contrast increases. To be sure that this trend was due to the inhomogeneity and not to boundary effects, we prepared and tested a homogeneous sample with a thickness of 3.6 cm. The results for the homogeneous problem, also shown in Fig. 4, show approximately constant contrast across the region of interest, convincing us that trends in the contrast ratio are due to the inhomogeneity and not to boundary effects. The contrast ratio for the inhomogeneous data approaches that for the homogeneous case as the distance from the center line increases, as one would expect. The variation in the two experimental curves for the inhomogeneous case and the ripple in the homogeneous data represent a measure of accuracy; the variations can likely be attributed to positioning precision and associated small inhomogeneities in the plastic. Multiple measurements at a fixed position show little change in contrast.

Also plotted in Fig. 4 is a numerically calculated contrast ratio as a function of source–detector scan position, achieved by use of Eq. (21) with $p(l)$ calculated with MUDPACK. A Gaussian fit to the measured power spectral density was used as $S(\lambda)$ in the calculations. The mesh size for the computational domain was chosen small enough to provide a convergent solution. The 3.6 cm $\times$ 15 cm $\times$ 15 cm domain was decomposed into $49 \times 97 \times 97$ cells. Boundary conditions were chosen by use of Eq. (31) with $n = 1.49$ for the plastic, resulting in a reflection, r_d, of 59%. The material parameters used in the simulation for the more highly scattering inhomogeneity were obtained from a series of contrast ratio measurements with varying thicknesses[19]; $\mu_a = 0.005\ \mathrm{cm}^{-1}$ and $\mu_s' = 40\ \mathrm{cm}^{-1}$ were used. The scattering parameters for the background were obtained with a fitting optimization procedure, in which contrast as a function of position for the inhomogeneous scan data was evaluated with a number of μ_a and μ_s' values. The background parameters that gave the best fit, and those used to produce the simulation result in Fig. 4, are $\mu_a = 0.01\ \mathrm{cm}^{-1}$ and $\mu_s' = 15\ \mathrm{cm}^{-1}$.

Figure 5 shows the calculated temporal impulse function for photon arrival times, with a scanned source–detector pair, for the case of a more highly scattering inhomogeneity. Two slices through the data of Fig. 5 are shown in Fig. 6 for points on the center line and at 24.74 mm from the center. The influence of the more scattering inhomogeneity on these temporal impulse responses

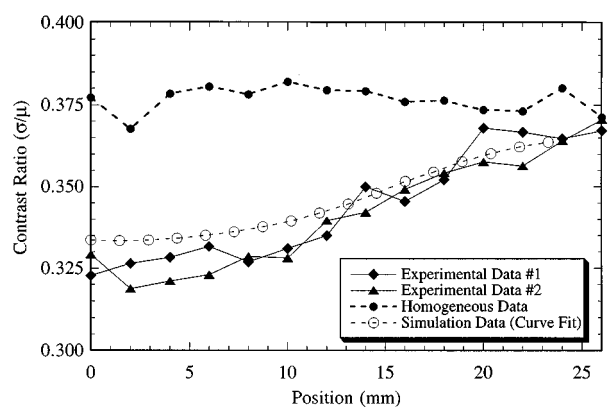

Fig. 4. Speckle intensity contrast (σ_I/μ_I) as a function of position for the more highly scattering inhomogeneity.

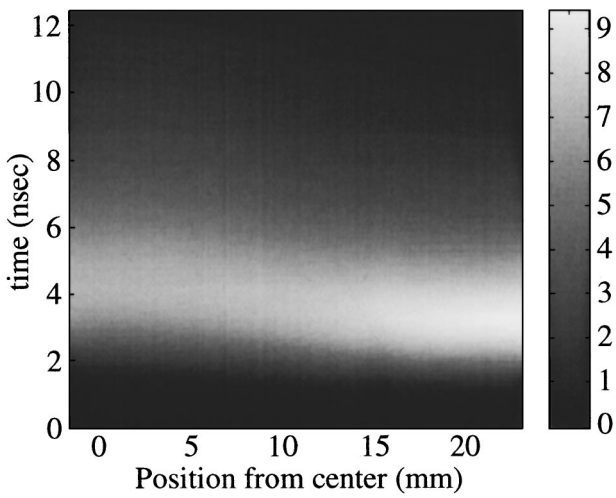

Fig. 5. Numerically simulated temporal impulse response as a function of scan position for the more highly scattering inhomogeneity.

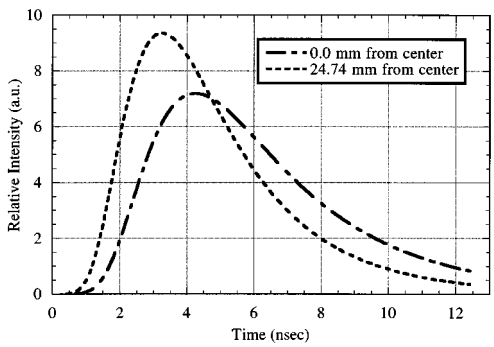

Fig. 6. Temporal impulse response for imaging points at the center line and at 2.474 cm from the center for denser inhomogeneity.

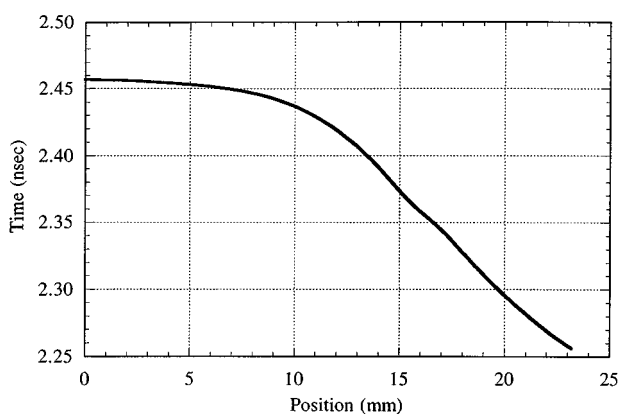

Fig. 7. Numerically computed characteristic time (σ_t) for the denser inhomogeneity.

(point-spread functions) is clear. Note that the characteristic time, σ_t, changes as the medium is translated, being larger when the transport is dominated by the more highly scattering region. The characteristic time-versus-scanning position is separately plotted in Fig. 7. As the characteristic time increases, implying more scattering events and a greater path length, the speckle contrast reduces. The characteristic time is still reducing at 23 mm from the center, indicating that the inhomogeneity is still influencing the speckle at that point. As the scan distance from the center line increases, the characteristic time will become constant and then reduce further because of its proximity to the free-space boundary.

With a fixed laser power and, for the present, uniform loss throughout both materials, higher scatter (larger effective μ_s') will cause the light to disperse more and consequently reduce the mean intensity at $\rho = 0$. Varying μ_a will compound this situation; in the materials used the μ_a are small and differ by only a factor of 2. For the case of a more highly scattering central inhomogeneity this trend is evident in the measured mean intensity as a function of scan position from the center line in Fig. 8. Also shown in this figure is the integral of the nonnormalized temporal impulse response, T in Eq. (25) [between times where the amplitude of $T(t)$ is 0.5% of the peak], scaled to the measured speckle intensity mean at the reference zero position. We expected the variation of the integral of $T(t)$ with scan position, which is a measure of total power, to be similar to that for the measured mean intensity, as it is.

Given the ability to detect denser inhomogeneities, we next performed the same experiment by replacing the more highly scattering inhomogeneity with a less scattering clear medium, a piece of clear Plexiglas. The background material remained the same as in the first example ($\mu_a = 0.01\ \mathrm{cm}^{-1}$ and $\mu_s' = 15\ \mathrm{cm}^{-1}$). In the ideal case the clear Plexiglas has infinite mean free path; in modeling such a region the diffusion equation does not hold. To simplify modeling by allowing the diffusion equation to be used throughout the domain, we assumed light scatter in the central region. In the MUDPACK simulations, $\mu_a = 0.01\ \mathrm{cm}^{-1}$ and $\mu_s' = 1.0\ \mathrm{cm}^{-1}$ were used.

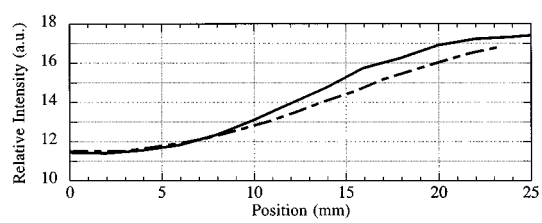

Fig. 8. Experimental mean intensity (solid curve) and scaled integral of the temporal impulse (dashed curve) response versus scanning position for the denser inhomogeneity.

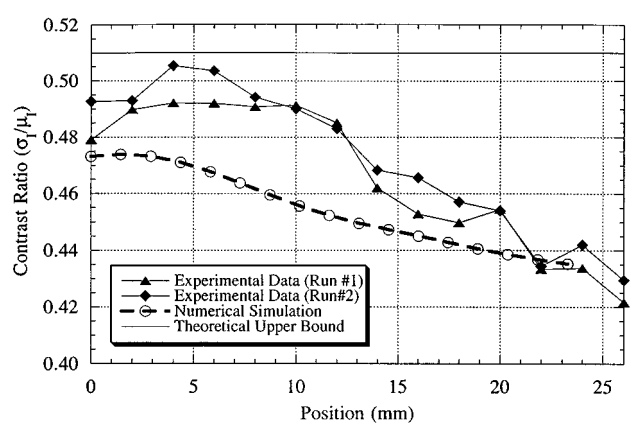

Fig. 9. Speckle intensity contrast as a function of scan position for the clear inhomogeneity.

A $97 \times 97 \times 97$ grid with the same boundary conditions as in the previous case was used. Again, we performed the experiment by scanning the plastic assembly while keeping the source and the detector fixed. The results comparing the experimental and numerical intensity contrast ratio as a function of scan position from the center line are presented in Fig. 9. As expected, when the inhomogeneity is centered the speckle contrast is maximum, trailing off from the homogeneous medium limit as the source–detector is scanned off center. The homogeneous limit is given as a computed value for 2.4 cm of background material (as if the center were removed and the material collapsed together) and appears as a constant curve at $\sigma_I/\mu_I = 0.51$ in Fig. 9. The discrepancy between the theory and experiment is due to the breakdown of the diffusion equation model in the clear region.

5. CONCLUSION

We have demonstrated a means of extracting information about the presence and location of inhomogeneities within highly scattering media by using speckle statistics with a partially coherent source. The temporal impulse response of the medium, calculated through use of the diffusion equation, was used to provide a probability-density function that corresponds to photon travel times, or path lengths, through the scattering medium. For an infinite homogeneous slab sample, the density function is independent of position along the output surface when the source and the detector are scanned in tandem. When an inhomogeneity is placed inside an otherwise homogeneous medium, the density function for path length becomes distorted from the uniform case. This disturbance can be detected by the speckle contrast method described when the coherence length of the source is comparable with the standard deviation of photon path lengths through the medium.

The plastics used were conveniently available. They were not chosen to provide special features such as high absorption. The differences between the highly scattering and the background plastic were really quite subtle.

Depending on the scattering parameters of the medium of interest, it might be necessary or advantageous to change the bandwidth of the light source. In addition to the technique presented here, in which speckle contrast is measured for a fixed laser coherence length, several other speckle imaging modalities should be possible. As an example, one could perform experiments in which the laser bandwidth is modulated to modify its coherence length.

In the medical imaging application, in which there could be appreciable motion of the medium over the measurement times that we have used thus far, a faster, time-gated speckle measurement would be necessary. Given that such a gate is used, the approach that we have outlined should be applicable. Speckle imaging and modulated light optical diffusion imaging represent different candidate approaches for obtaining images based on μ_a and μ_s' in the diffusion equation. Each technique has a variety of possible equipment components and implementations. The preferable approach will likely depend on the specific application.

The concepts demonstrated here may also find nonoptical applications, for example, in microwave and acoustic (sonar, ultrasound) measurements.

APPENDIX A

The intensity mean and standard deviation at the detector plane are related to those quantities at the image spot on the output plane of the scattering medium, and it is shown that, given certain approximations, the contrast ratio at the image spot is identical to that at the detector plane.

With Eq. (23), the field autocorrelation is

$$\Gamma_{U_d}(x, y, \lambda, \lambda') = \langle [U(x_i, y_i, \lambda) * K(x, y, x_i, y_i, \lambda)] \times [U^*(x_i, y_i, \lambda') * K^*(x, y, x_i, y_i, \lambda')] \rangle, \quad \text{(A1)}$$

where (x, y) designates the spatial variables in the detector plane and (x_i, y_i) those in the image plane. Equation (A1) can be written as[28]

$$\Gamma_{U_d}(x, y, \lambda, \lambda') = \langle U(x_i, y_i, \lambda) U^*(x_i, y_i, \lambda') \rangle * [K(x, y, x_i, y_i, \lambda) K^*(x, y, x_i, y_i, \lambda')]. \quad \text{(A2)}$$

From Eq. (7), when we substitute Γ_{U_d} rather than Γ_U, the mean in the detector plane is

$$\mu_{I_d}(x, y) = \int_0^\infty S(\lambda) \langle I_n(x_i, y_i, \lambda) \rangle * |K(x, y, x_i, y_i, \lambda)|^2 \mathrm{d}\lambda. \quad \text{(A3)}$$

As $\Delta\lambda/\lambda$ is small, K is independent of λ in the integration of Eq. (A3). Thus the detected mean is

$$\mu_{I_d}(x, y) = \mu_I(x_i, y_i) * |K(x, y, x_i, y_i)|^2. \quad \text{(A4)}$$

Applying Eq. (15) at the detector plane and using Eq. (A2) give

$$\sigma_{I_d}{}^2(x, y) = \int_0^\infty \int_0^\infty S(\lambda) S(\lambda') |\langle U_n(x_i, y_i, \lambda) \times U_n{}^*(x_i, y_i, \lambda') \rangle * [K(x, y, x_i, y_i, \lambda) \times K^*(x, y, x_i, y_i, \lambda')]|^2 \mathrm{d}\lambda \mathrm{d}\lambda'. \quad \text{(A5)}$$

$\mu_I(x_i, y_i)$ in Eq. (7) and $\sigma_I{}^2(x_i, y_i)$ in Eq. (15) are constant as (x_i, y_i) are varied within the small spot centered at (x_{i0}, y_{i0}) but vary with (x_{i0}, y_{i0}). The convolution in Eq. (A5) is with respect to the variables (x_i, y_i).

For $\Delta\lambda/\lambda$ small,

$$\langle U_n(x_i, y_i, \lambda) U_n{}^*(x_i, y_i, \lambda') \rangle = \langle I_n(x_i, y_i) \rangle \langle \exp\{-i[\phi(x_i, y_i, \lambda) - \phi(x_i, y_i, \lambda')]\} \rangle, \quad \text{(A6)}$$

where the expected values are constant over the image spot centered at (x_{i0}, y_{i0}). From Eq. (A5),

$$\sigma_{I_d}{}^2(x, y) = \int_0^\infty \int_0^\infty S(\lambda)S(\lambda')|\langle I_n(x_i, y_i)\rangle \times \langle \exp\{-i[\phi(x_i, y_i, \lambda) - \phi(x_i, y_i, \lambda')]\}\rangle * |K(x, y, x_i, y_i)|^2|^2 \mathrm{d}\lambda \mathrm{d}\lambda'. \tag{A7}$$

As $\langle I_n\rangle$ and $\langle \exp\{-i[\phi(\lambda) - \phi(\lambda')]\}\rangle$ are positive and independent of (x_i, y_i) over the image spot, Eq. (A7) can be written for a particular image spot at (x_{i0}, y_{i0}) as

$$\sigma_{I_d}{}^2(x, y) = \sigma_I{}^2 K_0{}^2(x, y), \tag{A8}$$

where $\sigma_I{}^2$ is given by Eq. (19) and $K_0{}^2$, for a particular image spot, is given by

$$K_0{}^2(x, y) = \left[\int\int_{x_i, y_i \in \mathrm{spot}} |K(x, y, x_i, y_i)|^2 \mathrm{d}x_i \mathrm{d}y_i\right]^2. \tag{A9}$$

From Eq. (A3),

$$\mu_{I_d}(x, y) = \mu_I K_0(x, y). \tag{A10}$$

Therefore, from Eqs. (A8) and (A10),

$$\frac{\sigma_{I_d}}{\mu_{I_d}} = \frac{\sigma_I}{\mu_I}. \tag{A11}$$

Equations (A3) and (A7) indicate that σ_{I_d} and μ_{I_d} vary with position (x, y) in the detector plane; i.e., they are nonstationary even if these quantities are constant within the image spot. However, provided that μ_I and σ_I are constant over an image spot at (x_{i0}, y_{i0}) and also that there is total rejection of light other than from the image spot, the contrast ratio at the detector plane is equal to that at the image plane.

*Now with Sensors and Communications Systems, Hughes Aircraft, El Segundo, California 90245-0902.

REFERENCES

1. J. G. Fujimoto, S. D. Silvestri, E. Ippen, C. Puliafito, R. Margolis, and A. Oseroff, "Eye-length measurement by interferometry with partially coherent light," Opt. Lett. **11**, 150–152 (1986).
2. E. Leith, C. Chen, H. Chen, Y. Chen, D. Dilworth, J. Lopez, J. Rudd, P. C. Sun, J. Valdmanis, and G. Vossler, "Imaging through scattering media with holography," J. Opt. Soc. Am. A **9**, 1148–1153 (1992).
3. M. R. Hee, J. A. Izatt, J. M. Jacobson, and J. G. Fujimoto, "Femtosecond transillumination optical coherence tomography," Opt. Lett. **18**, 950–952 (1993).
4. M. S. Patterson, B. Chance, and B. Wilson, "Time resolved reflectance and transmittance for the noninvasive measurement of tissue optical properties," Appl. Opt. **28**, 2331–2336 (1989).
5. J. B. Fishkin and E. Gratton, "Propagation of photon-density waves in strongly scattering media containing an absorbing semi-infinite plane bounded by a straight edge," J. Opt. Soc. Am. A **10**, 127–140 (1993).
6. J. S. Reynolds, S. Yeung, A. Przadka, and K. J. Webb, "Optical diffusion imaging: a comparative numerical and experimental study," Appl. Opt. **35**, 3671–3679 (1996).
7. H. Jiang, K. D. Paulsen, U. L. Osterberg, B. W. Pogue, and M. S. Patterson, "Optical image reconstruction using frequency domain data: simulations and experiments," J. Opt. Soc. Am. A **13**, 253–266 (1996).
8. D. G. Voelz, P. S. Idell, and K. A. Bush, "Illumination coherence effects in laser-speckle imaging," in *Laser Radar VI*, R. J. Becherer, ed., Proc. SPIE **1416**, 260–265 (1991).
9. R. Berkovits and S. Feng, "Theory of speckle-pattern tomography in multiple-scattering media," Phys. Rev. Lett. **65**, 3120–3123 (1990).
10. D. A. Boas, L. E. Campbell, and A. G. Yodh, "Scattering and imaging with diffusing temporal field correlations," Phys. Rev. Lett. **75**, 1855–1858 (1995).
11. P. Naulleau, D. Dilworth, E. Leith, and J. Lopez, "Detection of moving objects embedded within scattering media by use of speckle methods," Opt. Lett. **20**, 498–500 (1995).
12. J. D. Briers, "Speckle fluctuations and biomedical optics: implications and applications," Opt. Eng. **32**, 277–283 (1993).
13. G. Parry, "Some effects of temporal coherence on the first order statistics of speckle," Opt. Acta **21**, 763–772 (1974).
14. D. A. Zimnyakov, V. V. Tuchin, and S. R. Utts, "A study of statistical properties of partially developed speckle fields as applied to the diagnostics of structural changes in human skin," Opt. Spectrosc. (USSR) **76**, 838–844 (1994).
15. M. Rosenbluh, M. Hoshen, I. Freund, and M. Kaveh, "Time evolution of universal optical fluctuations," Phys. Rev. Lett. **58**, 2754–2757 (1987).
16. I. Freund, "Image reconstruction through multiple scattering media," Opt. Commun. **86**, 216–227 (1991).
17. A. Z. Genack, "Optical transmission in disordered media," Phys. Rev. Lett. **58**, 2043–2046 (1987).
18. A. Z. Genack and J. M. Drake, "Relationship between optical intensity fluctuations and pulse propagation in random media," Europhys. Lett. **11**, 331–336 (1990).
19. C. A. Thompson, K. J. Webb, and A. M. Weiner, "Diffusive media characterization using laser speckle," Appl. Opt. **36**, 3726–3734 (1997).
20. J. W. Goodman, "Statistical properties of laser speckle patterns," in *Laser Speckle and Related Phenomena*, 2nd ed., J. C. Dainty, ed., Vol. 9 of Topics in Applied Physics (Springer-Verlag, Berlin, 1984).
21. M. Born and E. Wolf, *Principles of Optics* (Pergamon, Oxford, 1980), p. 316.
22. I. S. Reed, "On a moment theorem for complex Gaussian processes," IRE Trans. Inf. Theory **8**, 194–195 (1962).
23. J. C. Adams, "MUDPACK: multigrid portable FORTRAN software for the efficient solution of linear elliptic partial differential equations," Appl. Math. Comput. **34**, 113–146 (1989).
24. J. C. Adams, *Multigrid Software for Elliptic Partial Differential Equations* (National Center for Atmospheric Research, Boulder, Colo., 1991).
25. R. A. J. Groenhuis, H. A. Ferwerda, and J. J. T. Bosch, "Scattering and absorption of turbid materials determined from reflection measurements. 1: Theory," Appl. Opt. **22**, 2456–2462 (1983).
26. W. G. Egan and T. W. Hilgeman, *Optical Properties of Inhomogeneous Materials* (Academic, New York, 1979).
27. S. E. Orchard, "Reflection and transmission of light by diffusing suspensions," J. Opt. Soc. Am. **59**, 1584–1597 (1969).
28. A. Papoulis, *Probability Random Variables and Stochastic Processes* (McGraw-Hill, New York, 1984), p. 272.